Carbohydrate Polymers 117 (2015) 778–787

Contents lists available at ScienceDirect

Carbohydrate Polymers

journal homepage: www.elsevier.com/locate/carbpol

Alkali-treated konjac glucomannan film as a novel wound dressing

Yi-Cheng Huang[a,*], Hao-Wen Chu[a], Chih-Ching Huang[b], Wen-Ching Wu[a], Jenn-Shou Tsai[a]

[a] Department of Food Science, College of Life Science, National Taiwan Ocean University, Keelung 20224, Taiwan
[b] Institute of Bioscience and Biotechnology, National Taiwan Ocean University, Keelung 20224, Taiwan

ARTICLE INFO

Article history:
Received 4 July 2014
Received in revised form 15 October 2014
Accepted 16 October 2014
Available online 31 October 2014

Keywords:
Konjac glucomannan
Alkali
Wound dressing

ABSTRACT

To investigate the potential medical application of konjac glucomannan (KGM), we treated KGM film with potassium hydroxide (KOH) or calcium hydroxide ($Ca(OH)_2$), and evaluated its use as a wound dressing. The $Ca(OH)_2$-treated KGM ($Ca(OH)_2$-KGM) film exhibited more favorable properties of swelling, tensile strength, and elongation compared with the KOH-treated KGM (KOH–KGM) film, and also had a suitable water vapor transmission rate. Results from in vitro 3-(4,5-dimethylthiazol-2-yl)-2,5-diphenyltetrazolium bromide assay further indicated the biocompatibility of the $Ca(OH)_2$-KGM film with L929 fibroblast cells and HaCaT keratinocyte cells. The $Ca(OH)_2$-KGM film inhibited the absorption and activation of platelets, and effectively promoted wound contractility in vivo, particularly at an early healing stage. Histological examination revealed considerably collagen secretion and advanced development of granulation tissue and epithelial coverage by Days 7 and 14 postsurgery in wounds treated with $Ca(OH)_2$-KGM film. Our study results indicate the potential use of alkali-treated KGM film as a novel wound dressing.

1. Introduction

Konjac glucomannan (KGM) is a natural polysaccharide derived from the tubers of *Amorphophallus konjac* K. Koch (Chua et al., 2012). KGM forms thermostable gels in certain conditions and is considered safe (Nishinari, Williams, & Phillips, 1992). It is composed of mannose and glucose in a molar ratio of 1.6:1, with β-1,4 linkages and acetyl groups randomly attached to the saccharide units along the molecule (Li, Xie, & Kennedy, 2011). Previous studies have modified the properties of KGM through alkaline deacetylation (Cheng, Abd Karim, Norziah, & Seow, 2002; Herranz, Tovar, Solo-de-Zaldivar, & Borderias, 2012; Pan, Meng, & Wang, 2011), which triggers gelation (Williams et al., 2000). Deacetylation of KGM causes acetyl-free regions of the backbone to associate, leading to the formation of junction zones and a three-dimensional network (Pan, He, & Wang, 2008).

In the food industry, KGM is an extensively used additive approved by the Food and Drug Administration (Herranz et al., 2012; Iglesias-Otero, Borderias, & Tovar, 2010). The biomedical application of KGM, such as in drug delivery systems (Alvarez-Mancenido, Landin, Lacik, & Martinez-Pacheco, 2008; Liu, Fan, Wang, & He, 2007; Yu, Lu, & Xiao, 2007) and cellular therapy (Slepian & Massia, 2001), has recently attracted attention. Ye et al. (2006) first used a chitosan-KGM film for fibroblast culturing (Ye, Kennedy, Li, & Xie, 2006). When KGM is added to chitosan materials, biocompatibility improves (Nie et al., 2011), indicating that KGM could be applied in tissue engineering. KGM has properties of heat stability, adjustable elasticity, and high transmittance, and represents a promising material for stimulating cellular metabolic activity through specific sugar receptors on fibroblasts. KGM hydrogels developed using free radical polymerization are candidates for application in wound healing (Shahbuddin, MacNeil, & Rimmer, 2012). However, few studies have evaluated the use of KGM-based materials in wound dressings.

In this study, we investigated the effects of alkalis on KGM film properties, such as degree of swelling, tensile strength (TS), and water vapor transmission rate (WVTR), and evaluated the potential use of the alkali-treated KGM films as wound dressings. We treated KGM films with potassium hydroxide (KOH) or calcium hydroxide ($Ca(OH)_2$) in various concentrations. Subsequently, we used texture analysis and scanning electron microscopy (SEM) to examine the structural and physicochemical properties of the alkali-treated KGM films. We evaluated biocompatibility by using 3-(4,5-dimethylthiazol-2-yl)-2,5-diphenyltetrazolium

* Corresponding author. Tel.: +886 2 2462 2192x5119; fax: +886 2 2463 4203.
E-mail addresses: ychuang@mail.ntou.edu.tw, d91548006@ntu.edu.tw (Y.-C. Huang).

http://dx.doi.org/10.1016/j.carbpol.2014.10.047
0144-8617/

bromide (MTT) and LIVE/DEAD assays, and by observing cell morphology. Our study results indicate the potential use of alkali-treated KGM films as wound dressings.

2. Materials and methods

Konjac glucomannan (KGM, Mw: 1000–1200 kDa) with 90% purity was supplied by Shimizu Chemical Co. (Japan). Calcium hydroxide ($Ca(OH)_2$) and potassium hydroxide (KOH) were purchased from Avantor Performance Materials (USA). All other chemicals were of reagent grade and were purchased from Sigma (St. Louis, MO, USA) unless stated otherwise.

2.1. KGM film preparation

KGM was dissolved in distilled water to a concentration of 1.6% (w/v). After swelling at room temperature for 20 min, $Ca(OH)_2$ or KOH was added to KGM solution with different weight ratios including 1.5% (w/w), 2.5% (w/w), and 3.5% (w/w). Next, the $Ca(OH)_2$/KGM or KOH/KGM solution were cast onto polystyrene plates and dried at 60 °C for 12 h. A series of $Ca(OH)_2$ treated KGM ($Ca(OH)_2$-KGM) films and KOH treated KGM (KOH–KGM) films were obtained and then stored in a dry environment until use.

2.2. Characterization of KGM film

The physical chemical properties of KGM film were examined as follows. The appearance of KGM film was observed with digital camera. For swelling behavior test, the films were cut into 1 cm × 1 cm with a thickness of 100 μm for drying in oven to constant weight (W_o). Then, the films were incubated in phosphate buffered saline (PBS) at room temperature for absorbing water to constant weight (W_t). The swelling degree in PBS was calculated using the following equation:

$$\text{Swelling degree}\,(\%) = \frac{Wt - Wo}{Wo} \times 100\%$$

The tensile strength (TS) and elongation (E) at break of the films were measured on an Instron apparatus (Model TA-XT2, Stable micro Ltd., USA). The samples, 1 cm × 6 cm, were cut from each film. Initial grip separation and crosshead speed were set at 30 mm and 3 mm/s, respectively. TS and E were calculated following the formula below:

$$\text{Tensile strength}\quad (\text{TS}) = \frac{F}{S}$$

$$\text{Elongation}\,(\text{E}, \%) = \frac{L_i - L_o}{L_o} \times 100\%$$

$F_{(\text{N})}$: maximum stress of stretching; $S_{(\text{mm}^2)}$: initial sectional area of sample; L_o: initial sample length; L_i: sample length at breakage ($n = 4$).

The water vapor transmission rate (WVTR) of the films was determined using the standard method stipulated by the American Society for Testing and Materials standard method. The KGM films (30 mm × 30 mm in size) were 100-μm thick and were mounted on the mouths of cylindrical plastic cups (25 mm in diameter) containing 10 mL of distilled water in an incubator at 37 °C for 24 h. The WVTRs were calculated using the following equation:

$$\text{WVTR} = \frac{W2 - W1}{A} \times 10^6\ \text{gm}^{-2}\text{day}^{-1}$$

where the WVTR is expressed in $\text{gm}^{-2}\,\text{day}^{-1}$, A (mm^2) is the bottle mouth area, and W_2(g) and W_1(g) are the weights of the films before and after being placed in the incubator, respectively.

2.3. Biocompatibility evaluation

To evaluate the biocompatibility of KGM films, cell viability was measured using an MTT assay (Sigma-Aldrich, St. Louis, MO, USA) according to manufacturer instructions. The L929 fibroblast cells (1.0×10^5 cells/well) or HaCaT keratinocyte cells (1.0×10^5 cells/well) were planted in 24-well plates on which KGM film have been coated. After culturing for 24 h, 48 h and 72 h, respectively, the MTT (100 mg/mL, 1000 μL) was then added to each well and incubated at 37 °C for 4 h. After cautiously aspirating the culture medium, 500 μL of dimethyl sulfoxide (DMSO) was added and thoroughly mixed for 10 min. Absorbance was determined at 570 and 630 nm usnig a microplate spectrophotometer (SpectraMax 340PC^{384}, Molecular Devices, Sunnyvale, CA, USA). Moreover, LIVE/DEAD Viability/Cytotoxicity Kit (Invitrogen, USA) was used for examining live and dead cells. The morphology of cells on KGM films was observed by scanning electron microscopy (SEM, JEOL Ltd.). Cells grown on tissue culture polystyrene (TCP) were used as the control.

2.4. Platelet absorption test

The platelet concentrate was prepared from blood drawn from a human body. The KGM films sterilized with 75% ethanol for 24 h were placed on a 24-well bottom. Each well was added with platelet concentrate (density: $1.9 \times 10^5\ \mu\text{L}^{-1}$), and incubated at 37 °C for 120 min. The SEM was used to observe the morphology of the platelets absorbed on the KGM films. Glass was used as positive control (Lee, Chen, & Tsao, 2010)

2.5. In vivo wound healing experiments

This study was conducted in accordance with Guide for the Care and Use of Laboratory Animals. The Animal Care and Use Committee of National Taiwan Ocean University approved all procedures that involved animals. The animal ethical permission registration number is 102056. Male Sprague-Dawley rats (SD rats, 250–400 g) were used for the study. After they were anesthetized with Zoletil with dose of 50 mg/kg of body weight, the back was shaved with standard animal clippers, and skin was swabbed with 70% ethanol, a mid-line excision was performed in the back and the animal was exposed with a stainless steel retractor. Full thickness skin defect with round shape of 2 cm diameter was made on the animals' back parallel to the vertebral column. The wound sites were marked and measured using digital calipers and averaged to determine the original wound diameter and area. The wound was then dressed with (1) Tegaderm$^{\text{TM}}$ (3 M Health Care, St. Paul, MN) (control group) or (2) $Ca(OH)_2$-KGM film and Tegaderm$^{\text{TM}}$ (named as $Ca(OH)_2$-KGM group).

Wound closure observation of each animal was assessed by tracing the wound with digital camera on days 3, 7, 10 and 14 post-wounding surgery. The wound closure rate was expresses as the following equation:

$$\text{Wound closure}\quad (\%) = \frac{A_o - A_i}{A_o} \times 100\%$$

where A_o is the orignial wound area; A_i is the wound area at specified time point. The wounds and the surrounding skin post-operation for day 7 and 14 were fixed with 10% formaldehyde solution, paraffin embedded and stained with hematoxylin and eosin (H&E) reagent for histological examinations. Furthermore, the Masson's trichrome stain was used to observe the formation and distribution of collagen (stained blue) on the wounds. For quantitative analysis, the regenerated tissues was recorded by an inverted light microscope (Best Scope, BS-7000B, China) and then analyzed by Image J software.

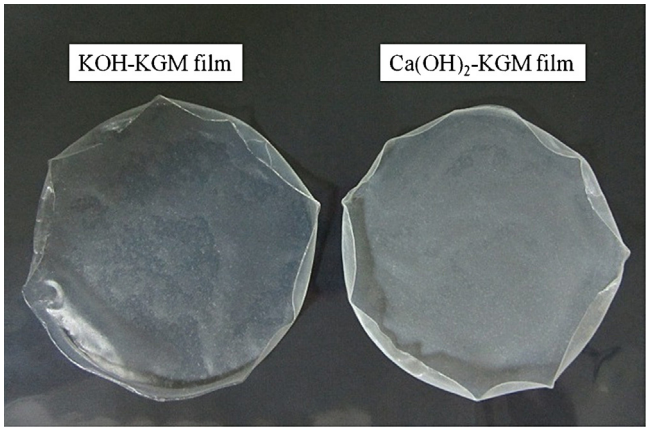

Fig. 1. Photographic appearance of (A) KOH–KGM film and (B) $Ca(OH)_2$-KGM film.

2.6. Statistical analysis

All quantitative data are expressed as mean ± standard deviation (SD). Statistical analysis was by one-way ANOVA and the post-test was performed using GraphPad Prism 5; $P < 0.05$ was considered statistically significant.

3. Results and discussion

3.1. Characterization of KGM film

The $Ca(OH)_2$-KGM and KOH–KGM films were both transparent (Fig. 1). The thickness of the film was 100 μm. Fig. 2A displays the changes in pH values observed after soaking the alkali-treated KGM films in double-distilled water (ddH_2O). Ten minutes postimmersion, the KOH–KGM film had considerably increased the pH of the ddH_2O to 9.33, which is unfavorable for cell growth. By contrast, when we immersed the $Ca(OH)_2$-KGM film in ddH_2O for 30 min, the pH remained at approximately 7.5. This experimental result could be related to salt solubility. The degree of solubility of a salt is governed by equilibrium and is indicated by the solubility product constant, Ksp. KOH is a strong electrolyte with a higher Ksp value than that of $Ca(OH)_2$ at room temperature. Excess hydroxide ions (OH^-) might have reprecipitated with calcium cations (Ca^{2+}) to reduce the pH of the $Ca(OH)_2$-KGM solution. For the KOH–KGM solution, the release of OH^- might have caused the high pH value.

Fig. 2B shows the degree of swelling in the alkali-treated KGM film according to various alkali/KGM ratios. The KOH–KGM and $Ca(OH)_2$-KGM films both exhibited strong water uptake capabilities (>300%), which is essential in wound dressings for rapid absorption of exudates. High water absorptive ability results from strong interactions between water molecules and OH groups (in the KGM film) (Fan et al., 2013). The swelling behaviors of the KOH–KGM and $Ca(OH)_2$-KGM films were similar, with decreasing degree of swelling associated with increasing amount of alkali. These effects could be attributed to alkaline deacetylation of KGM molecules, causing more extensive intermolecular interaction (Cheng et al., 2002). Alkaline deacetylation of the KGM polymer reduces steric hindrance and increases polymer chain association. Increased intermolecular interaction might reduce the number of sites for water sorption. We observed a marginally higher degree of swelling in the KOH–KGM film than in the $Ca(OH)_2$-KGM film, which could have been caused by a higher hydration number for potassium cations (K^+) than Ca^{2+} (Jalilehvand et al., 2001; Mahler & Persson, 2012).

When we evaluated the mechanical properties of the alkali-treated films, we observed that the highest TS of the $Ca(OH)_2$-KGM and KOH–KGM films was 3.5 ± 0.3 MPa and 2.9 ± 0.4 MPa, respectively (Fig. 2C). Alkali-treated KGM film is suitable for application as a wound dressing because of TS in the range of 2.5–16 MPa (Ezequiel, Edel, Alexandra, Wander, & Herman, 2009). TS increased considerably with increasing amount of alkali (per KGM film) from 1.5% (w/w) to 2.5% (w/w), and remained almost constant until the amount of alkali reached 3.5% (w/w). The $Ca(OH)_2$-KGM film exhibited a higher TS than the KOH–KGM film did. Increased TS following

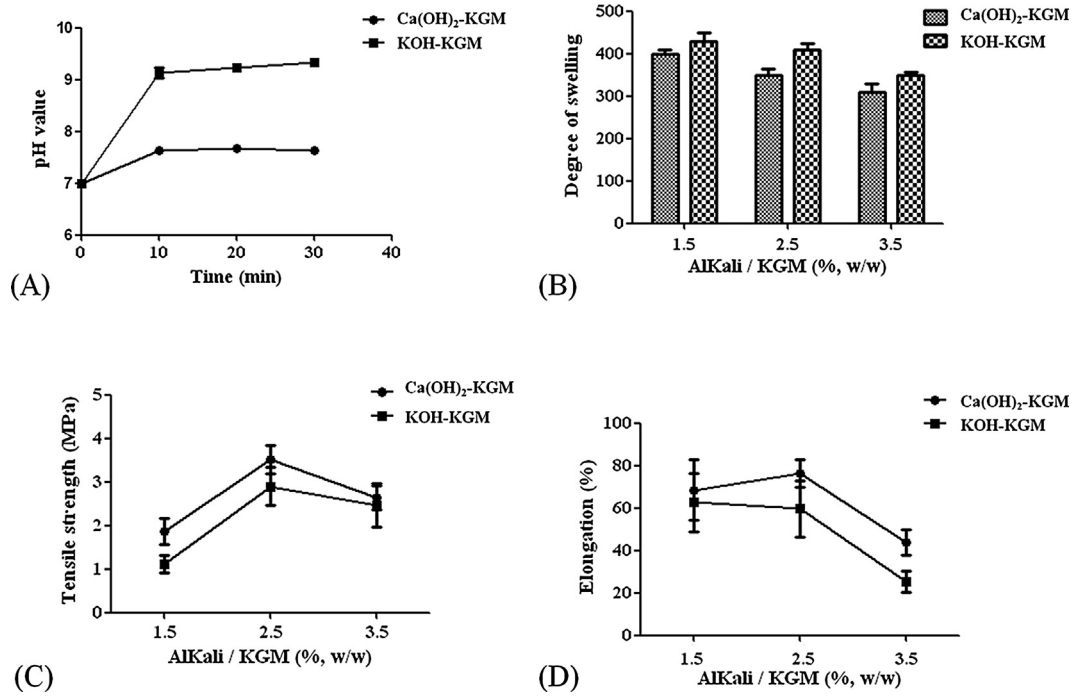

Fig. 2. The physical-chemical properties of KOH–KGM and $Ca(OH)_2$-KGM films. (A) The pH value after immersing films in ddH_2O (B) swelling degree (C) tensile strength (D) elongation. Data are presented by the mean ± SD, $n = 4$.

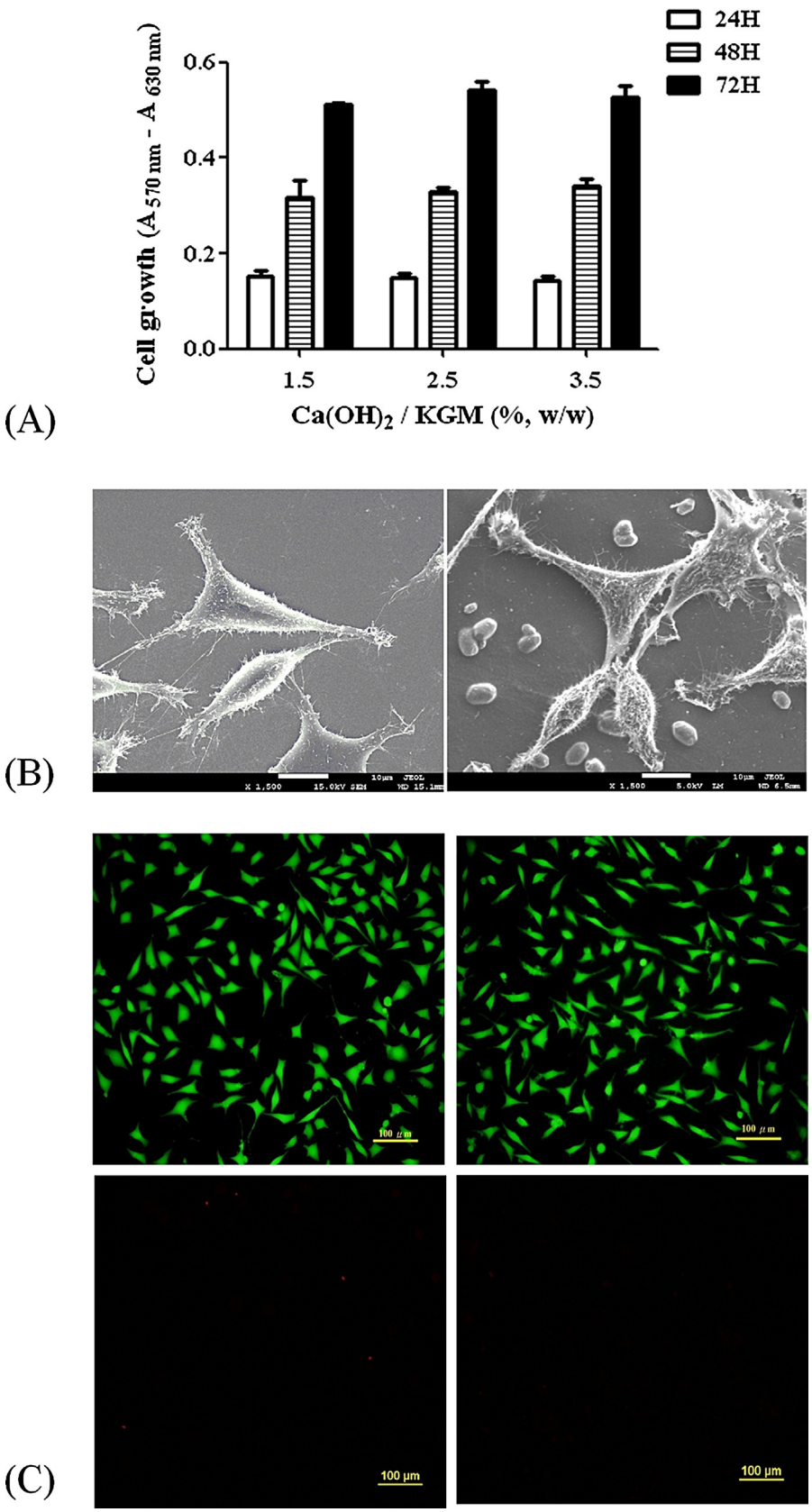

Fig. 3. In vitro biocompatibility test of $Ca(OH)_2$-KGM film to L929 fibroblast cells. (A) Cell growth measured by MTT assay. (B) Attachment and (C) fluorescence images of L929 fibroblast cells on TCP (left) and $Ca(OH)_2$-KGM film (right). Green and red fluorescent stains are representatives of live and dead cells, respectively. (For interpretation of the references to color in this figure legend, the reader is referred to the web version of this article.)

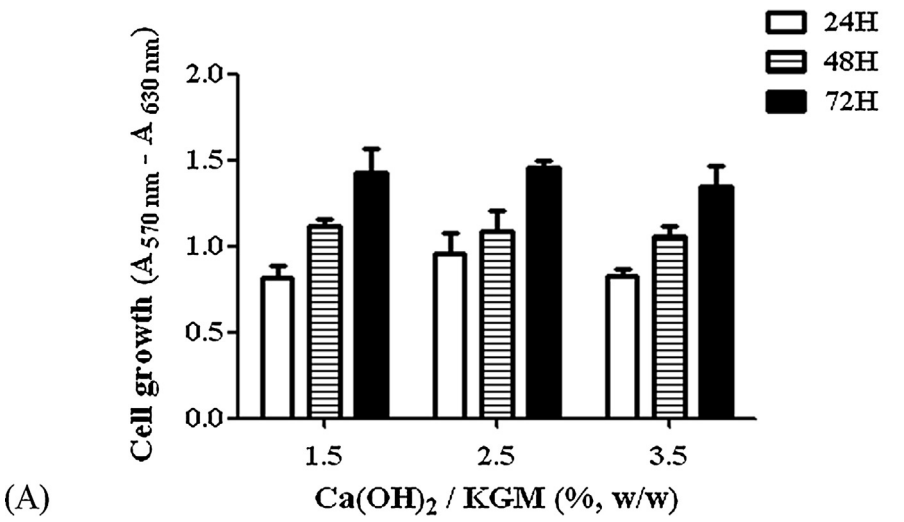

(A)

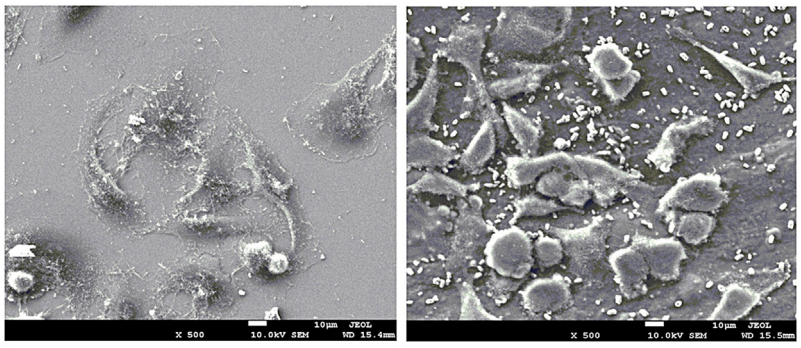

(B)

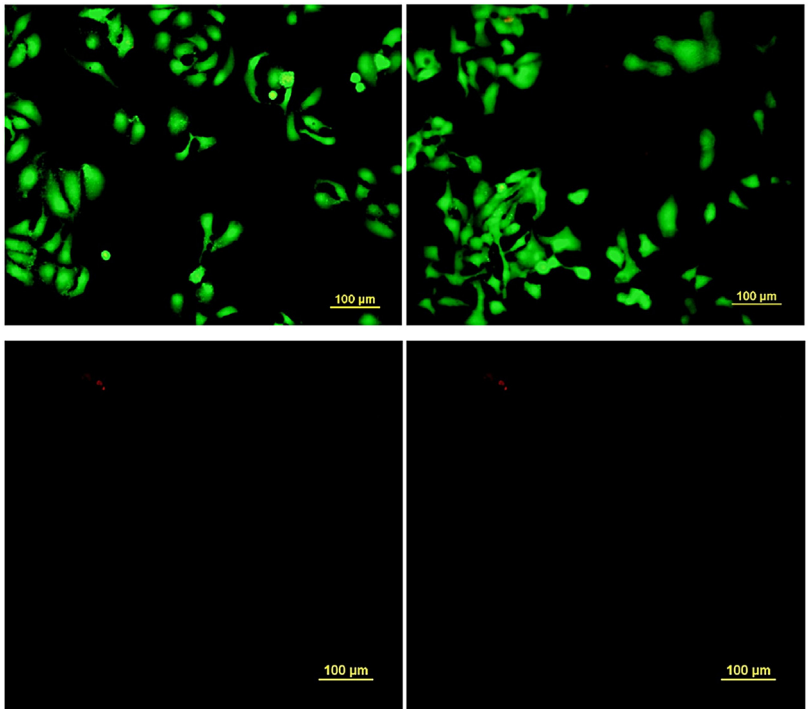

(C)

Fig. 4. In vitro biocompatibility test of $Ca(OH)_2$-KGM film to HaCaT keratinocyte cells. (A) Cell growth measured by MTT assay. (B) Attachment and (C) fluorescence images of HaCaT keratinocyte cells on TCP (left) and $Ca(OH)_2$-KGM film (right). Green and red fluorescent stains are representatives of live and dead cells, respectively. (For interpretation of the references to color in this figure legend, the reader is referred to the web version of this article.)

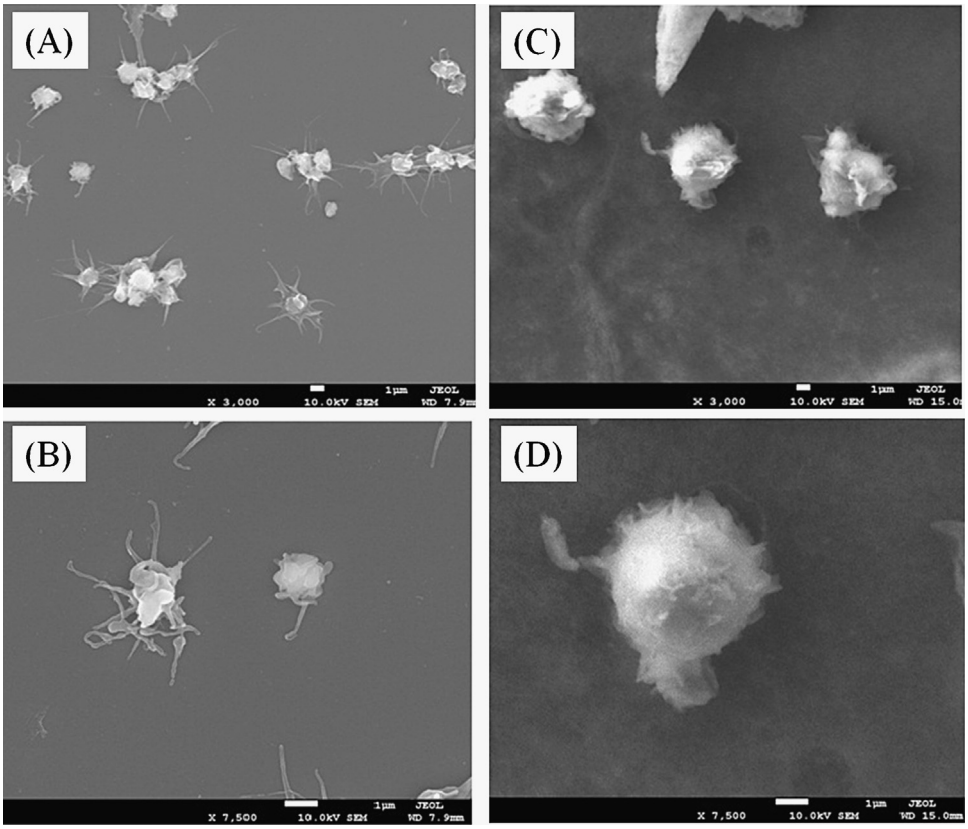

Fig. 5. The morphology of platelets absorbed on the surface of (A, B) Glass and (C, D) $Ca(OH)_2$-KGM film. Magnifications: (A, C) ×3000; (B, D) ×7500.

the addition of alkali is caused by alkaline deacetylation of KGM to promote intermolecular interaction through hydrogen bonding, leading to the formation of a more highly structured matrix (Cheng et al., 2002; Jin et al., 2014; Pan et al., 2011). Ion-dipole interactions might have caused marginally higher TS in the $Ca(OH)_2$-KGM film than in the KOH–KGM film. Ca^{2+} has a denser electrostatic charge (more positive charges within the same radius) than K^+ do because of divalency. Ca^{2+} is thus associated with stronger ion-dipole interactions with water molecules and with OH groups of KGM chains, producing a higher level of dipolar order in the network compared with K^+ (Herranz et al., 2012).

The $Ca(OH)_2$- and KOH-treated KGM films exhibited the same trends in breaking elongation. Elongation decreased considerably when the amount of alkali increased from 2.5% (w/w) to 3.5% (w/w) (Fig. 2D). We observed more extensive elongation in the $Ca(OH)_2$-KGM film than in the KOH–KGM film. According to these physical-chemical properties, we selected the $Ca(OH)_2$-KGM film for subsequent analyses.

As shown in Table 1, the water vapor transmission rate (WVTR) of the $Ca(OH)_2$-KGM film ranged from 2027.4 ± 67.6 to $2069.4 \pm 60.8\ g m^{-2}\ day^{-1}$. Typically, wound dressings with a WVTR between 2000 and $5000\ g m^{-2}\ day^{-1}$ prevent excess dehydration of wound surfaces, avoid excess accumulation of exudate, and maintain a wet wound environment (Kim et al., 2007). Our experimental results indicated that our $Ca(OH)_2$-KGM film can provide a moist wound environment and effectively prevent water evaporation.

Table 1
Water vapor transmission rate of $Ca(OH)_2$-KGM film.

$Ca(OH)_2$/KGM (%, w/w)	WVTR ($g m^{-2}\ day^{-1}$)
1.5	2047.7 ± 68.4
2.5	2069.4 ± 60.8
3.5	2027.4 ± 67.6

Data are presented by the mean ± SD, $n = 4$.

3.2. Attachment and growth of cells on KGM film

Fig. 3A shows our results from MTT assay, indicating KGM film biocompatibility with L929 fibroblast cells. The L929 fibroblast cells proliferated at approximately equal rates irrespective of the $Ca(OH)_2$/KGM ratio, as indicated by similarities in the slope of increasing absorbance. We observed extended filopodias on L929 fibroblast cells attached on the $Ca(OH)_2$-KGM film (Fig. 3B). L929 fibroblast cell morphology was the same on the $Ca(OH)_2$-KGM film and in a TCP (control group). Fig. 3C shows our results from LIVE/DEAD assay. Green and red fluorescenct stains are representatives of live and dead cells, respectively. In the 72 h after cell seeding, we observed green-fluorescent spindles in the L929 fibroblast cells, indicating cell growth.

The growth of HaCaT keratinocyte cells on the $Ca(OH)_2$-KGM film positively correlated with culturing time (Fig. 4A). Fig. 4B shows our SEM results on HaCaT keratinocyte cell morphology after attachment to the $Ca(OH)_2$-KGM film. Fig. 4C shows our LIVE/DEAD assay results. Our results indicated that the $Ca(OH)_2$-KGM film exerted nontoxic effects on the attached HaCaT keratinocyte cells.

3.3. Platelet adhesion

When we used SEM to observe the surface of the $Ca(OH)_2$-KGM film and evaluate platelet adhesion, we observed that the average number of absorbed platelets on the $Ca(OH)_2$-KGM film under each view (7500×) was ≤1 (Fig. 5D), which was fewer than in the control group (glass) (Fig. 5B). SEM revealed that control group platelets had obvious pseudopods (Fig. 5A and B) (Mao et al., 2004), whereas the platelets on the $Ca(OH)_2$-KGM surface were absent

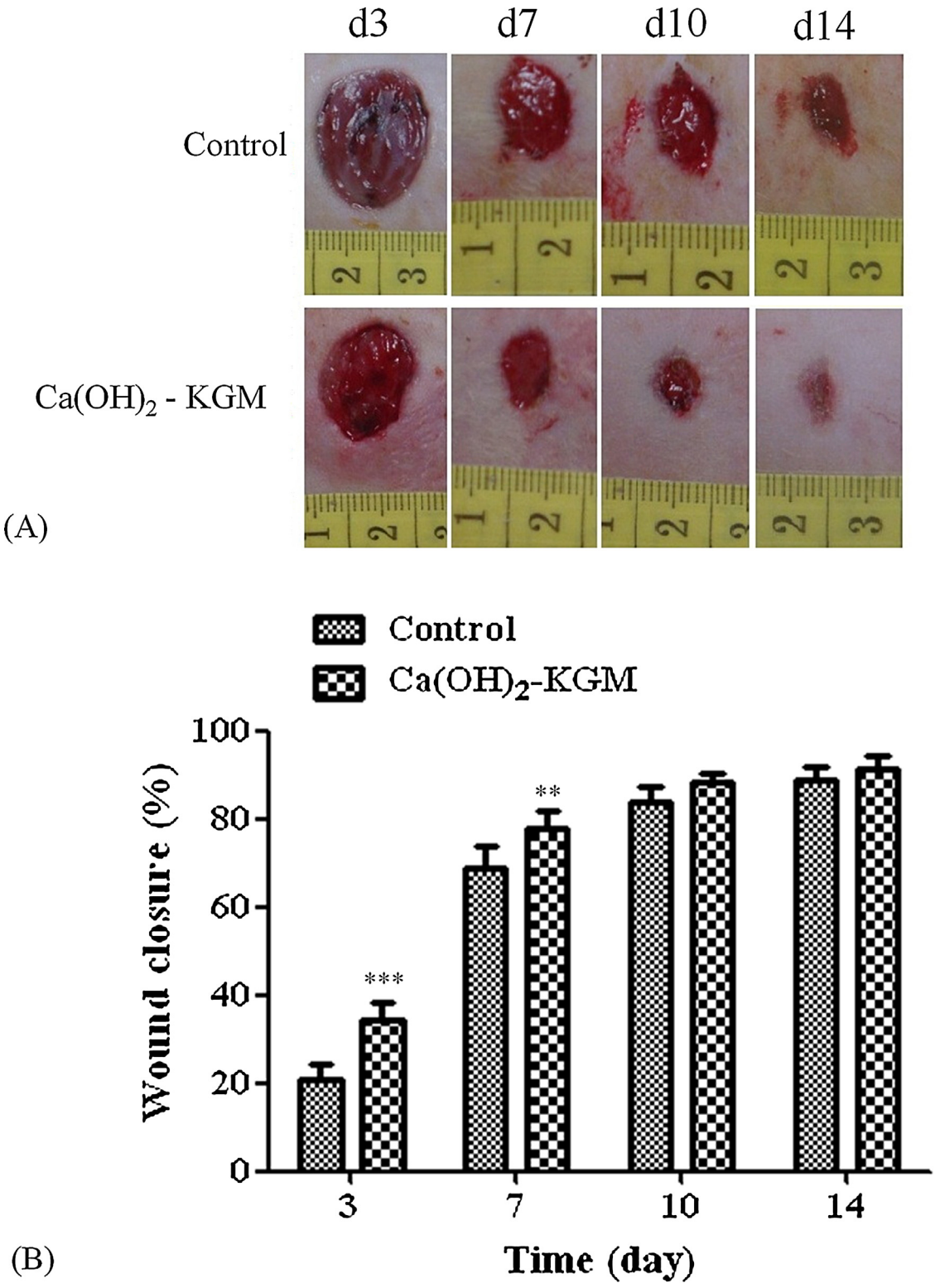

Fig. 6. (A) Photographs and (B) wound closure percentage of applying $Ca(OH)_2$-KGM film to full skin defects on SD rat. The quantitative data are represented by the mean ± SD, $n = 7$. ** $P < 0.01$ versus control; *** $P < 0.001$ versus control.

of pseudopods (Fig. 5C and D). These results indicated that the $Ca(OH)_2$-KGM film is inert to platelets and resists their absorption.

3.4. *In vivo animal tests*

To observe wound healing in vivo, we placed $Ca(OH)_2$-KGM film on SD rat wound sites 3, 7, 10, and 14 days postsurgery. Fig. 6A shows photographs of wound closure postoperatively and Fig. 6B presents the quantitative data. Three days postsurgery, we observed considerable exudate resulting in a wet wound in the control group. In the $Ca(OH)_2$-KGM group, we observed a healthy clean pink-red wound with moderate wettability without wound-soaking. The wound closure percentage in the control and $Ca(OH)_2$-KGM film groups exhibited significant differences. Seven

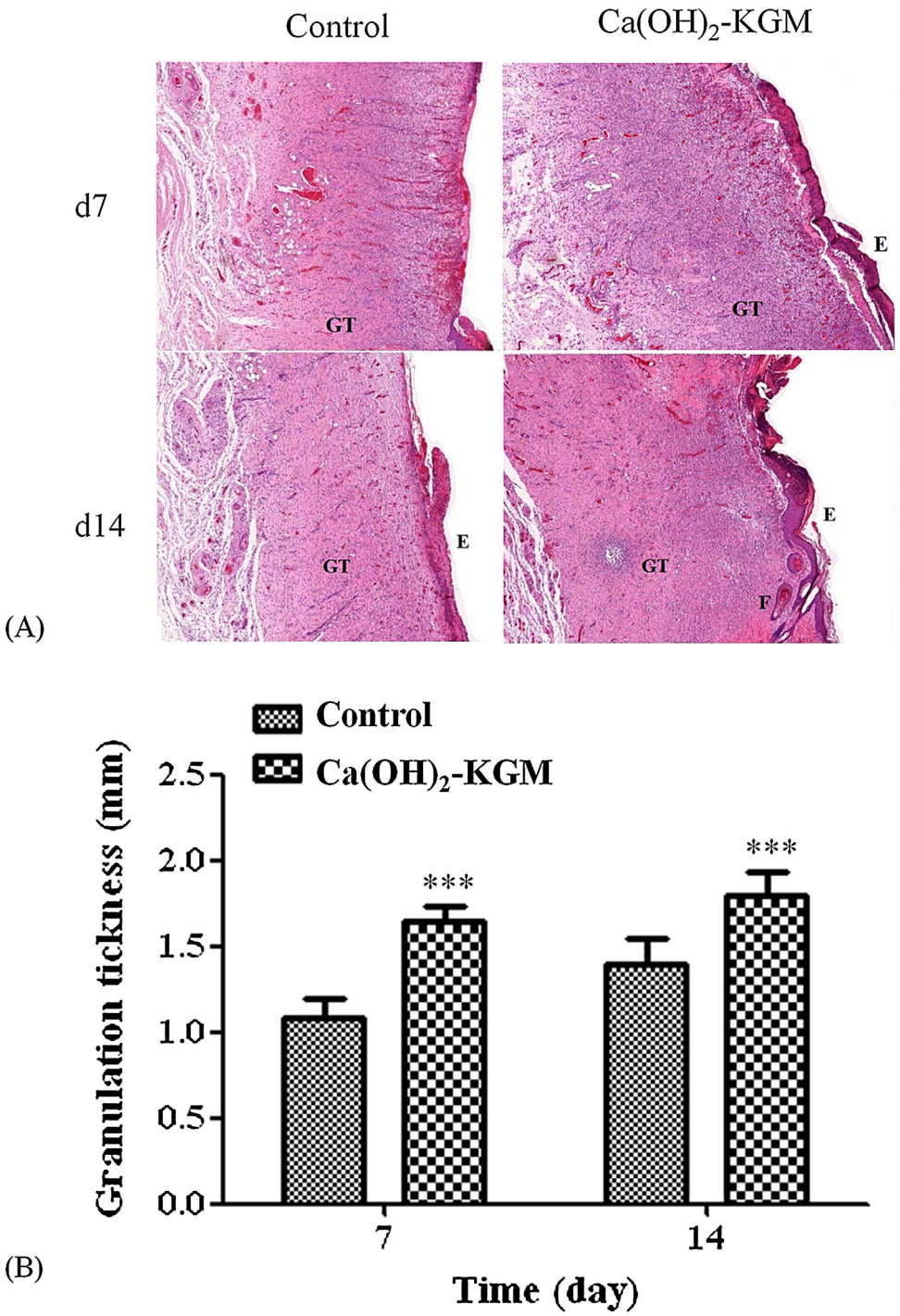

Fig. 7. (A) Mircographs and (B) granulation tissue formation of full skin wounds 7 d and 14 d post-surgery. The quantitative data are represented by the mean ± SD, $n = 5$. *** $P < 0.001$ versus control. GT: Granulation tissue; (E): Epidermis; (F): Hair follicles.

days postsurgery, the wound of the control group excreted exudate continuously, which prolonged the healing process. The $Ca(OH)_2$-KGM dressing maintained wound moistness, with no accumulation of exudate and no signs of inflammation or infection. A higher wound closure percentage in the $Ca(OH)_2$-KGM group compared with in the control group indicated the ability of the $Ca(OH)_2$-KGM film to promote wound contractility. Epithelialization can be accelerated by maintaining a wet wound environment and avoiding exudate accumulation (Junker, Kamel, Caterson, & Eriksson, 2013; Winter & Scales, 1963). The WVTR of the $Ca(OH)_2$-KGM film was approximately 2000 gm^{-2} day^{-1} (Table 1), which is reportedly suitable for maintaining a moist wound surface and facilitates epidermal cell migration (Kim et al., 2007). Fourteen days postsurgery, the majority of the wound tissue had repaired in both groups, with no obvious residual scar tissue.

Histological analysis by H&E staining indicated the promoting effects of the $Ca(OH)_2$-KGM film on wound healing (Fig. 7). By Day 7 postsurgery, we observed substantially greater epithelial coverage in the $Ca(OH)_2$-KGM group compared with in the control group. Fourteen days postsurgery, we observed the complete reepithelialization of wounds in the $Ca(OH)_2$-KGM group. The granulation tissue of the wound gradually thickened with time.

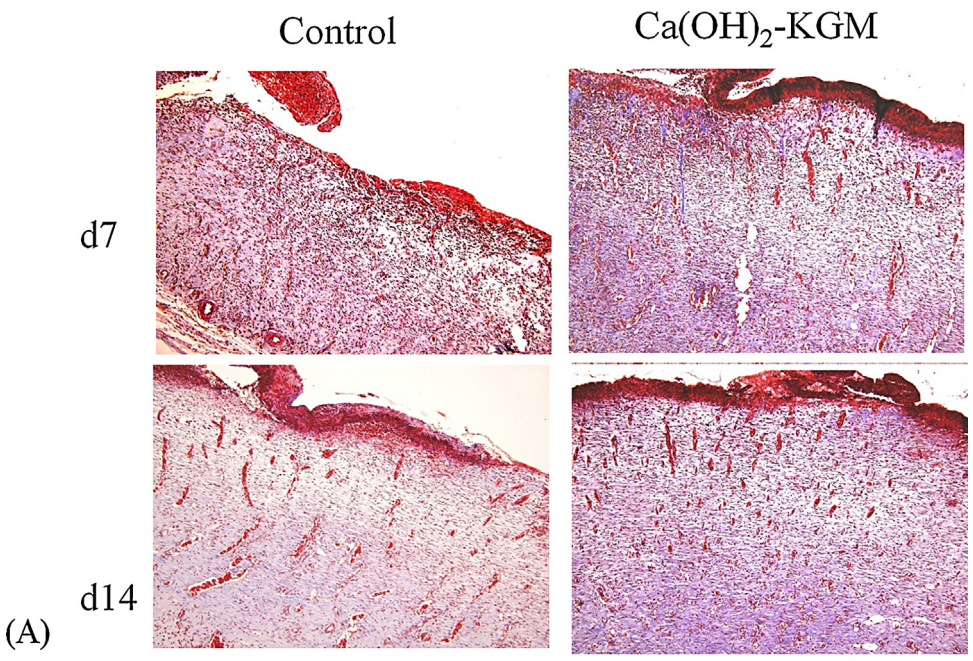

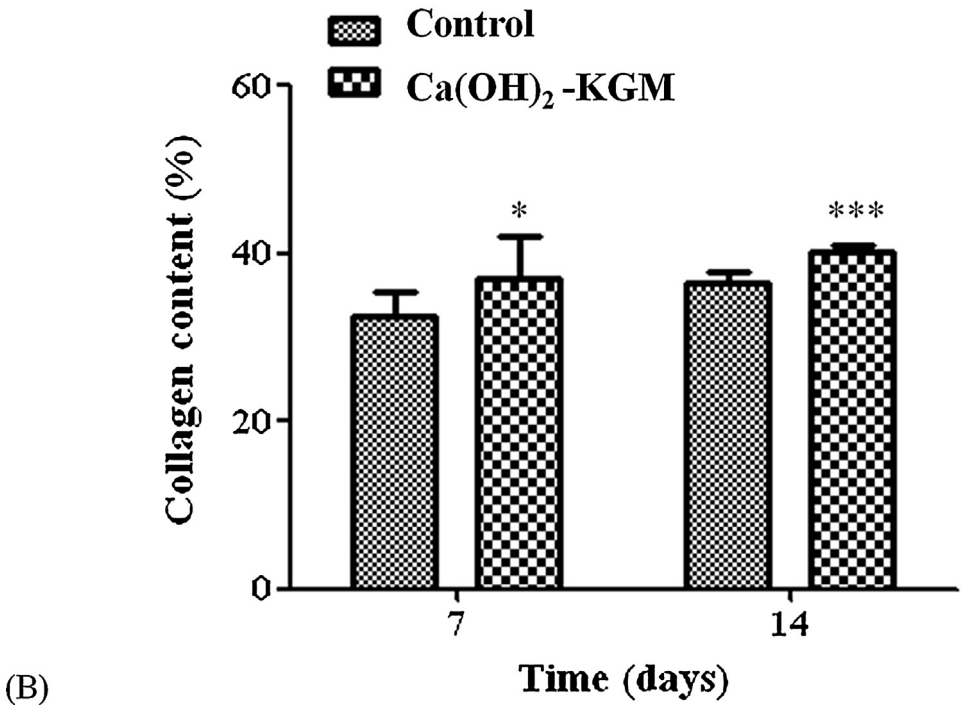

Fig. 8. (A) Mircographs and (B) collagen formation of full skin wounds 7 d and 14 d post-surgery (Masson's trichrome stain). The quantitative data are represented by the mean ± SD, $n = 5$. * $P < 0.05$ versus control; *** $P < 0.001$ versus control.

The $Ca(OH)_2$-KGM group exhibited thicker granulation tissue and more extensive development of hair follicles compared with the control group. Acceleration of wound contraction and reepithelialization in the $Ca(OH)_2$-KGM wounds indicated improvement in the overall healing process.

The extracellular ground substances of skin tissues predominantly contain type 1 collagen. We used Masson's trichrome (MT) staining to identify collagen (Li et al., 2008) and determine the distribution of extracellular ground substances in the regenerated tissues. The color intensity (blue) in the tissue sections indicated the relative quantity of collagen. As shown in Fig. 8, the intensity of MT staining indicated that the amount of collagen secreted increased with time in the control and $Ca(OH)_2$-KGM groups. However, we observed higher wound collagen content overall in the $Ca(OH)_2$-KGM group compared with in the control group. The color intensity values of the two groups exhibited significant differences, suggesting that the $Ca(OH)_2$-KGM group secreted larger amounts of collagen than the control group did (Fig. 8B).

4. Conclusion

This study evaluated the feasibility of using KOH- and $Ca(OH)_2$-treated KGM films as biomaterials for wound healing. The alkali-treated KGM films exhibit suitable chemical-physical properties for use as wound dressings, good biocompatibility, and effectively accelerate wound repair. Our experimental results indicate that the $Ca(OH)_2$-KGM film has more favorable properties of TS, elongation, and degree of swelling than the KOH–KGM film does. The $Ca(OH)_2$-KGM film also exhibits a suitable WVTR for use as a wound dressing. The $Ca(OH)_2$-KGM film is compatible with L929 fibroblast cells, HaCaT keratinocyte cells, and blood, and accelerates wound contraction and reepithelialization processes. In conclusion, $Ca(OH)_2$-KGM films can potentially be used as dressings to promote wound healing.

Acknowledgments

The authors would like to thank the National Science Council of Taiwan for financially supporting this research under contract no. NSC 102-2221-E-019-004. Thanks to Ms. C.-Y. Chien of Ministry of Science and Technology, Taiwan for the assistance in SEM experiments. Wallace Academic Editing is appreciated for his editorial assistance.

References

Alvarez-Mancenido, F., Landin, M., Lacik, I., & Martinez-Pacheco, R. (2008). Konjac glucomannan and konjac glucomannan/xanthan gum mixtures as excipients for controlled drug delivery systems. Diffusion of small drugs. *International Journal of Phamaceutics*, *349*(1-2), 11–18.

Cheng, L. H., Abd Karim, A., Norziah, M. H., & Seow, C. C. (2002). Modification of the microstructural and physical properties of konjac glucomannan-based films by alkali and sodium carboxymethylcellulose. *Food Research International*, *35*(9), 829–836.

Chua, M., Chan, K., Hocking, T. J., Williams, P. A., Perry, C. J., & Baldwin, T. C. (2012). Methodologies for the extraction and analysis of konjac glucomannan from corms of *Amorphophallus konjac* K. Koch. *Carbohydrate Polymers*, *87*(3), 2202–2210.

Ezequiel, S. C. J., Edel, F. B. S., Alexandra, A. P. M., Wander, L. V., & Herman, S. M. (2009). Preparation and characterization of chitosan/poly(vinyl alcohol) chemically crosslinked blends for biomedical applications. *Carbohydrate Polymers*, *76*, 472–481.

Fan, L., Cheng, C., Qiao, Y., Li, F., Li, W., Wu, H., et al. (2013). GNPs-CS/KGM as hemostatic first aid wound dressing with antibiotic effect: In vitro and in vivo study. *PLoS One*, *8*(7), e66890.

Herranz, B., Tovar, C. A., Solo-de-Zaldívar, B., & Borderias, A. J. (2012). Effect of alkalis on konjac glucomannan gels for use as potential gelling agents in restructured seafood products. *Food Hydrocolloids*, *27*(1), 145–153.

Iglesias-Otero, M. A., Borderias, J., & Tovar, C. A. (2010). Use of konjac glucomannan as additive to reinforce the gels from low-quality squid surimi. *Journal of Food Engineering*, *101*(3), 281–288.

Jalilehvand, F., Spangberg, D., Lindqvist-Reis, P., Hermansson, K., Persson, I., & Sandstrom, M. (2001). Hydration of the calcium ion. An EXAFS, large-angle x-ray scattering, and molecular dynamics simulation study. *Journal of the American Chemical Society*, *123*(3), 431–441.

Jin, W., Mei, T., Wang, Y., Xu, W., Li, J., Zhou, B., et al. (2014). Synergistic degradation of konjac glucomannan by alkaline and thermal method. *Carbohydrate Polymers*, *99*, 270–277.

Junker, J. P., Kamel, R. A., Caterson, E. J., & Eriksson, E. (2013). Clinical impact upon wound healing and inflammation in moist, wet, and dry environments. *Advances in Wound Care (New Rochelle)*, *2*(7), 348–356.

Kim, I. Y., Yoo, M. K., Seo, J. H., Park, S. S., Na, H. S., Lee, H. C., et al. (2007). Evaluation of semi-interpenetrating polymer networks composed of chitosan and poloxamer for wound dressing application. *International Journal of Phamaceutics*, *341*(1–2), 35–43.

Lee, M. W., Chen, H. J., & Tsao, S. W. (2010). Preparation, characterization and biological properties of Gellan gum films with 1-ethyl-3-(3-dimethylaminopropyl)carbodiimide cross-linker. *Carbohydrate Polymers*, *82*(3), 920–926.

Li, B., Xie, B. J., & Kennedy, J. F. (2011). Studies on the molecular chain morphology of konjac glucomannan (Retraction of vol 64, pg 510, 2006). *Carbohydrate Polymers*, *86*(3), 1421.

Li, H., Fu, X., Zhang, L., Huang, Q., Wu, Z., & Sun, T. (2008). Research of PDGF-BB gel on the wound healing of diabetic rats and its pharmacodynamics. *Journal of Surgical Research*, *145*(1), 41–48.

Liu, M., Fan, J., Wang, K., & He, Z. (2007). Synthesis, characterization, and evaluation of phosphated cross-linked konjac glucomannan hydrogels for colon-targeted drug delivery. *Drug Delivery*, *14*(6), 397–402.

Mahler, J., & Persson, I. (2012). A study of the hydration of the alkali metal ions in aqueous solution. *Inorganic Chemistry*, *51*(1), 425–438.

Mao, C., Zhu, J. J., Hu, Y. F., Ma, Q. Q., Qiu, Y. Z., Zhu, A. P., et al. (2004). Surface modification using photocrosslinkable chitosan for improving hemocompatibility. *Colloids and Surfaces B: Biointerfaces*, *38*(1–2), 47–53.

Nie, H. R., Shen, X. X., Zhou, Z. H., Jiang, Q. S., Chen, Y. W., Xie, A., et al. (2011). Electrospinning and characterization of konjac glucomannan/chitosan nanofibrous scaffolds favoring the growth of bone mesenchymal stem cells. *Carbohydrate Polymers*, *85*(3), 681–686.

Nishinari, K., Williams, P. A., & Phillips, G. O. (1992). Review of the physico-chemical characteristics and properties of konjac mannan. *Food Hydrocolloids*, *6*, 199–222.

Pan, Z., Meng, J., & Wang, Y. (2011). Effects of alkalis on deacetylation of konjac glucomannan in mechano-chemical treatment. *Particuology*, *9*, 265–269.

Pan, Z. D., He, K., & Wang, Y. M. (2008). Deacetylation of konjac glucomannan by mechanochemical treatment. *Journal of Applied Polymer Science*, *108*(3), 1566–1573.

Shahbuddin, M., MacNeil, S., & Rimmer, S. (2012). Synthesis and preparation of konjac glucomannan hydrogel for wound healing. *Journal of Tissue Engineering and Regenerative Medicine*, *6*(Suppl. 1), 1–429.

Slepian M.J., & Massia S.P. (2001). Local polymeric gel cellular therapy, United States Patent (Patent no.: US6290729 B1).

Williams, M. A., Foster, T. J., Martin, D. R., Norton, I. T., Yoshimura, M., & Nishinari, K. (2000). A molecular description of the gelation mechanism of konjac mannan. *Biomacromolecules*, *1*(3), 440–450.

Winter, G. D., & Scales, J. T. (1963). Effect of air drying and dressings on the surface of a wound. *Nature*, *197*, 91–92.

Ye, X., Kennedy, J. R., Li, B., & Xie, B. J. (2006). Condensed state structure and biocompatibility of the konjac glucomannan/chitosan blend films. *Carbohydrate Polymers*, *64*(4), 532–538.

Yu, H., Lu, J., & Xiao, C. (2007). Preparation and properties of novel hydrogels from oxidized konjac glucomannan cross-linked chitosan for in vitro drug delivery. *Macromolecular Bioscience*, *7*(9–10), 1100–1111.